

Motility of efferent duct cilia aids passage of sperm cells through the male reproductive system

Isabella Aprea^{1,†}, Tabea Nöthe-Menchen^{1,†}, Gerard W. Dougherty¹, Johanna Raidt¹, Niki T. Loges¹, Thomas Kaiser¹, Julia Wallmeier¹, Heike Olbrich¹, Timo Strünker¹ ², Sabine Kliesch², Petra Pennekamp¹ ^{1,*}‡, and Heymut Omran¹ ^{1,*}‡

¹Department of General Pediatrics, University Hospital Muenster, Muenster 48149, Germany ²Department of Clinical Andrology, Centre of Reproductive Medicine and Andrology, University Hospital Muenster, Muenster 48149, Germany

*Correspondence address. University Hospital Muenster, Department of General Pediatrics, Albert-Schweitzer-Campus 1, building A1, Muenster 48149, Germany. E-mail: Heymut.Omran@ukmuenster.de;  <https://orcid.org/0000-0003-0282-6765>; University Hospital Muenster, Department of General Pediatrics, Albert-Schweitzer-Campus 1, Building A1, Muenster 48149, Germany; E-mail: Petra.Pennekamp@ukmuenster.de  <https://orcid.org/0000-0002-8202-3809>

Submitted on April 28, 2020; resubmitted on January 6, 2021; editorial decision on February 3, 2021

ABSTRACT: Motile cilia line the efferent ducts of the mammalian male reproductive tract. Several recent mouse studies have demonstrated that a reduced generation of multiple motile cilia in efferent ducts is associated with obstructive oligozoospermia and fertility issues. However, the sole impact of efferent duct cilia dysmotility on male infertility has not been studied so far either in mice or human. Using video microscopy, histological- and ultrastructural analyses, we examined male reproductive tracts of mice deficient for the axonemal motor protein DNAH5: this defect exclusively disrupts the outer dynein arm (ODA) composition of motile cilia but not the ODA composition and motility of sperm flagella. These mice have immotile efferent duct cilia that lack ODAs, which are essential for ciliary beat generation. Furthermore, they show accumulation of sperm in the efferent duct. Notably, the ultrastructure and motility of sperm from these males are unaffected. Likewise, human individuals with loss-of-function *DNAH5* mutations present with reduced sperm count in the ejaculate (oligozoospermia) and dilatations of the epididymal head but normal sperm motility, similar to *DNAH5* deficient mice. The findings of this translational study demonstrate, in both mice and men, that efferent duct ciliary motility is important for male reproductive fitness and uncovers a novel pathomechanism distinct from primary defects of sperm motility (asthenozoospermia). If future work can identify environmental factors or defects in genes other than *DNAH5* that cause efferent duct cilia dysmotility, this will help unravel other causes of oligozoospermia and may influence future practices in genetic and fertility counseling as well as ART.

Key words: efferent ducts / cilia / sperm / motor proteins / outer dynein arm-defects / DNAH5 / 45 male infertility / oligozoospermia / motile ciliopathy / primary ciliary dyskinesia

Introduction

Male fertility is compromised when sperm cells are reduced in number (oligozoospermia) or do not swim properly (asthenozoospermia). Both conditions occur in the majority of idiopathic cases of male infertility (Bracke et al., 2018), but the underlying causes still remain unknown in about 40% of affected individuals, despite several diagnostic efforts.

However, research has shown that astheno- and oligozoospermia associated male infertility are common in diseases characterized by impaired function of motile cilia, such as primary ciliary dyskinesia (PCD) (Munro et al., 1994). As motile cilia are known to perform a number

of essential functions, such as clearing the airways, circulating cerebrospinal fluid, and supporting the transport of the oocyte across the fallopian tube (Fliegauf et al., 2007; Raidt et al., 2015), it was taken for granted that motile ciliopathies would impair sperm motility, and thus lead to male infertility.

About 150 years ago, Becker and colleagues discovered that cells lining the efferent duct epithelium in the male reproductive tract harbor multiple motile cilia (Fig. 1). Despite intensive research, the functional role of efferent duct cilia motility in male fertility has remained controversial. Initially, it was assumed that the beating of these cilia transports the sperm from the testis into the epididymis (Becker, 1856). However, subsequent work, especially in mouse

[†]These authors should be regarded as joint First Authors.

[‡]These authors share the last authorship.

© The Author(s) 2021. Published by Oxford University Press on behalf of European Society of Human Reproduction and Embryology.

This is an Open Access article distributed under the terms of the Creative Commons Attribution Non-Commercial License (<http://creativecommons.org/licenses/by-nc/4.0/>), which permits non-commercial re-use, distribution, and reproduction in any medium, provided the original work is properly cited. For commercial re-use, please contact journals.permissions@oup.com

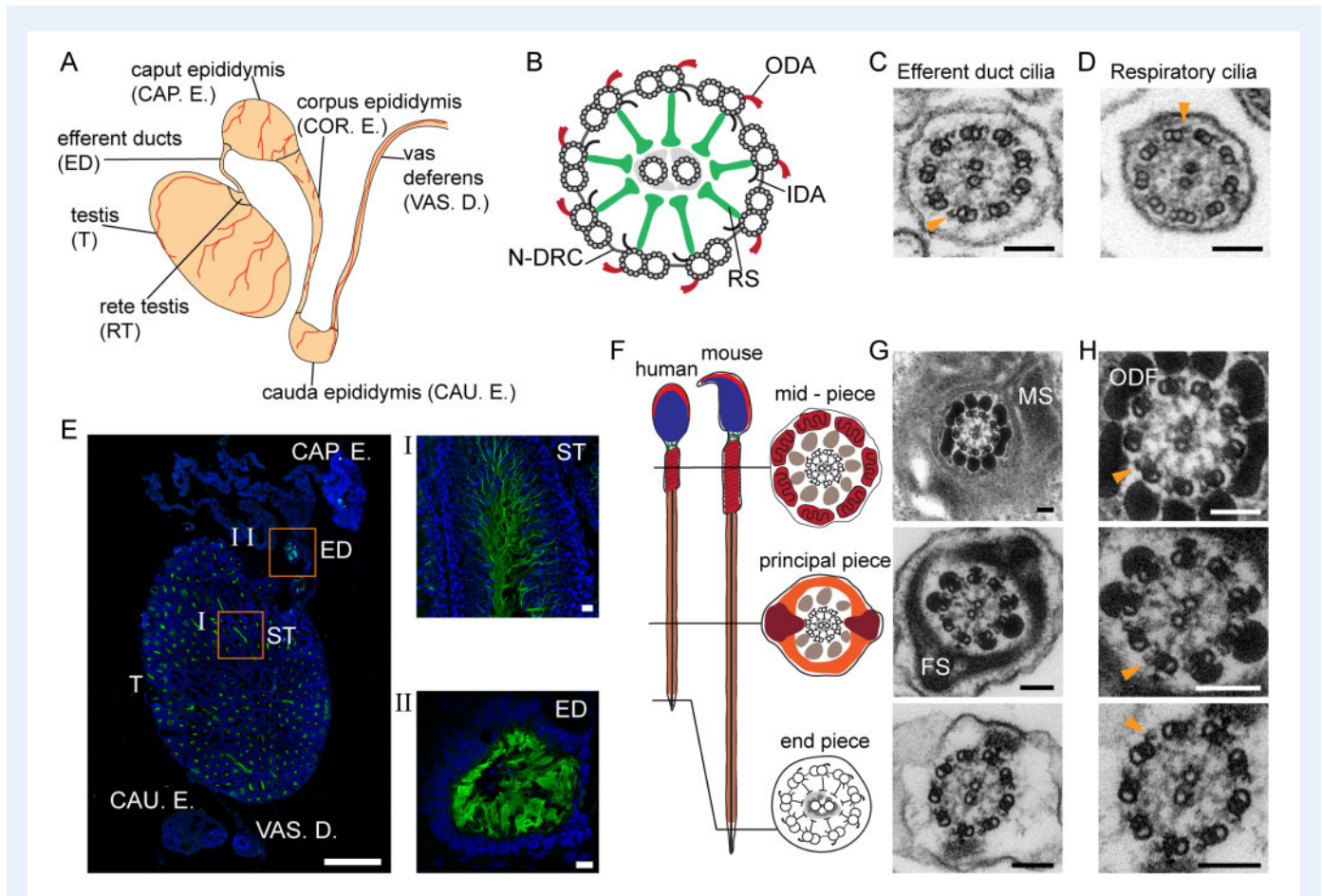


Figure 1. Cilia and flagella in the mouse male reproductive tract. **A**, overview of the mouse male reproductive tract. **B**, ciliary/flagellar axonemes consist of microtubules and functional complexes. ODA: outer dynein arm; IDA: inner dynein arm; RS: radial spoke; N-DRC: nexin-dynein regulatory complex. **C**, axoneme ultrastructure of control mouse efferent duct and **D**, respiratory cilia. **E**, IF labeling for acetylated alpha-tubulin (green; DAPI-labelled nuclei: blue) in the mouse male reproductive tract. (I) spermatozoa in seminiferous tubules (ST). (II) efferent duct cilia. Nuclei (blue) were stained with DAPI. **F**, schematic and **G**, TEM cross sections of sperm flagella with axonemes surrounded by accessory structures. **H**, detail of **G**. Biological replicate: $n=3$; Scale bars represent 100 nm (C, D, G and H), 1000 μm (E), 10 μm (I and II). **C**, **D**, **H**, orange arrowheads indicate ODAs.

models with reduced generation of motile efferent duct cilia, suggested a different function. According to these other studies, efferent duct cilia do, instead, stir the luminal seminiferous fluid to keep sperm in suspension, promote fluid reabsorption and avoid sperm from clogging during the passage to the epididymis (Hess et al., 1997; Hess, 2002; Danielian et al., 2016; Terré et al., 2019; Yuan et al., 2019).

In this study, we set out to elucidate whether dysmotility of efferent duct cilia alone represents a pathomechanism for male infertility, in both humans and mice. Throughout the animal kingdom, ciliary dysmotility and/or immotility occurs when motile cilia have defective axonemal outer dynein arms (ODAs) (Fliegauf et al., 2007; Spassky and Meunier, 2017). Thus, we reasoned that genetic defects affecting the ODA structure and function could also affect the motility of efferent duct cilia and possibly impact male fertility.

However, because several genetic deficiencies that impact ODA composition involve both motile cilia and sperm flagella (Omran et al.,

2008; Paff et al., 2017; Höben et al., 2018), we chose to study a genetic defect that exclusively disrupts the ODA composition of motile cilia but does not affect ODA composition and motility of sperm flagella.

To this end, we analyzed the impact of DNAH5 deficiency in the male reproductive system of *Mdnah5* (*Dnah5*^{Tg1Htz2}) mice by using histological and functional approaches. Furthermore, we assessed the fertility status in DNAH5 deficient PCD-affected men by detailed andrologic examinations and semen analyses. DNAH5 mutations are a common cause for PCD in human, associated with defects of the axonemal ODA motor complex required for cilia beat generation. Homozygous mutants of the *Mdnah5* mouse line (*Mdnah5*^{mut/mut}) do also lack the ODAs in respiratory epithelial cells and ependymal cells and reproduce a classical PCD phenotype (Ibanez-Tallon, 2002; Olbrich et al., 2002; Ibañez-Tallon et al., 2004; Hornef et al., 2006). We studied the male reproductive tract of this mouse line in order to elucidate the outcome of DNAH5 deficiency on the structure and

function of efferent duct cilia, because access to this tissue is limited for obvious reasons in humans.

Material and methods

Experimental design

The aim of this study was to characterize the specific role of ciliary motility in efferent ducts of the mammalian reproductive tract for the passage of sperm from the testis to the epididymis, and thus its role for male fertility. To this purpose, we aimed to analyse efferent duct cilia and their functional role in the *Dnah5^{Tg1Hz}* (referred to as *Mdnah5^{mut/mut}*) mouse model (Ibanez-Tallon, 2002) compared to wild type control littermates. *Mdnah5^{mut/mut}* mice, deficient for the axonemal motor protein DNAH5, lack ciliary ODA, essential for ciliary beat generation, and present dysmotile multiple motile cilia. Additionally, the fertility status of adult human males suffering from PCD owing to disease-causing mutations in *DNAH5* was examined in comparison to healthy control individuals. PCD individuals for this study were selected out of our patient cohort for motile ciliopathies, based on their gender, age (≥ 18 years), mutational status and clinical features characteristic for a *DNAH5* deficiency. For this explorative study, sample size pre-calculations were performed via a two-tailed Student's t-test using the statistical program G*Power version 3.1.9 (Faul et al., 2007; Erdfelder et al., 2009).

Mouse analyses

Characterization of efferent duct cilia was performed by analyzing three ($n = 3$) adult wild type I29Sv males. Furthermore, mouse analyses were performed on *Dnah5^{Tg1Hz}* mice (Ibanez-Tallon, 2002), backcrossed from a C57BL/6J strain to a I29Sv genetic background. In total, we investigated 11 homozygous mutant (*Mdnah5^{mut/mut}*) mice and nine wild type (*Mdnah5^{wt/wt}*) control littermates, with ages ranging from days postnatal (P) P7–P50. Mice that did not survive until adulthood (P7, P9, P10, P11, P12, P24, P25 and P30) and thus did not complete the first wave of spermatogenesis (Oakberg, 1956; Bellve et al., 1977; Laiho et al., 2013) were used for the examination of only efferent duct cilia. Examination of sperm structure and function and fertility was performed on three mice that survived until P40, P45 and P50, completing the first wave of spermatogenesis (Oakberg, 1956; Bellve et al., 1977; Laiho et al., 2013). Male reproductive tracts (from testis to vas deferens) were dissected after euthanasia of the animals through decapitation (P0–P14) or cervical dislocation ($>P14$) and used for different analyses, reducing the overall number of animals necessary. Owing to hydrocephalus formation in *Mdnah5^{mut/mut}* mice, for some analyses we could only analyze three adult homozygous mutant males (P40, P45 and P50). Mice were housed under specific-pathogen-free conditions in cages (according to EU-guideline 2010/63/EU) with bedding and nesting material containing up to five animals and monitored by qualified members of the working group. The housing temperature was 22–24°C constantly and a day and night light cycle (12:12h) was maintained. Water and food were available *ad libitum*. All mouse analyses met the requirements of ethical regulations and current European and German law (animal welfare act (Tierschutzgesetz) and animal welfare—laboratory animal regulation

(Tierschutz-Versuchstierverordnung)) and were approved by local government (Landesamt für Natur, Umwelt und Verbraucherschutz Nordrhein-Westfalen, Reference number: Az. 84-02.05.50.15.025; Az. 81-02.04.2018. A107).

Human samples

Ejaculate samples and respiratory cells from nasal brush biopsies were collected from both adult men with PCD and healthy control individuals ($n = 4$ /group). Blood for DNA isolation and genetic testing was obtained from individuals fulfilling the diagnostic criteria and from family members. All participating subjects gave written informed consent, and protocols have been approved by the Institutional Ethics Review Board at the University of Muenster (Muenster, Germany) (Reference number: Az. 2017-139-f-5).

Semen analysis

Semen analysis was conducted in the accredited andrology laboratory of the Centre for Reproductive Medicine and Andrology (CeRA), University Clinics, Münster (Germany), fulfilling latest World Health Organization (WHO) guidelines (World Health Organization, 2010) and was under constant internal and external quality control. These standards also fulfill the methodological criteria according to Björndahl et al. (2016). Semen of healthy volunteers and studied PCD individuals were collected by masturbation after 2–7 days of sexual abstinence and evaluated after liquefaction for 30 min at 37°C to assess, for example, the sperm cell concentration and motility. Remaining ejaculate of each individual was used for high-resolution immunofluorescence (IF)-, transmission electron- and high-speed video microscopy analyses.

Mutational analysis

Disease causing *DNAH5* mutations in PCD affected males were identified as previously described (Höben et al., 2018; Loges et al., 2018) by next generation sequencing techniques, such as a customized PCD gene panel and whole-exome sequencing, and verified by Sanger sequencing. Primers used for Sanger sequencing are listed in Supplementary Table S1. Genomic DNA was isolated by standard methods directly from blood samples.

High speed video microscopy analyses (HVMA)

Ciliary beat pattern was assessed in I29Sv wild type mouse efferent ducts ($n = 3$). Efferent duct ciliary beat frequency (CBF) ($n = 5$ *Mdnah5^{wt/wt}*; $n = 7$ *Mdnah5^{mut/mut}* mice) and the motility and viability of sperm cells ($n = 2$ /group) were further analyzed in adult *Mdnah5^{mut/mut}* mice (P45 and P50) and control siblings (P45 and P50). Male reproductive tracts, spanning regions from the testis to the vas deferens, were excised and washed in DMEM/F12 Medium, HEPES, without phenol red (Thermo Fischer Scientific, Waltham, MA, USA), supplemented with 10% fetal bovine serum (Thermo Fischer Scientific, Waltham, MA, USA). Efferent ducts were separated from the testis and caput epididymis and incised longitudinally to expose the ciliated epithelium. Sperm cells were obtained from the corpus epididymis by incision of this region followed by a stream out and/or swim up of sperm cells in 1 ml modified TYH medium (Mukherjee et al., 2016) (20 min, at 37°C and 5% CO₂). Dissected efferent ducts and sperm suspension were

analyzed at $\times 40$ and $\times 63$ magnification with an Eclipse Ti Inverted Microscope (Nikon, Tokyo, Japan) connected to an ES310 Turbo Megaplus High Speed Camera (Kodak, Rochester, NY, USA) at 37°C . Using the same instrumentation, $10\ \mu\text{l}$ of liquefied human ejaculate was analyzed to assess motility of sperm cells. Video analyses were performed with the Sisson-Ammons Video Analysis (SAVA) system (Sisson et al., 2003) and exported videos processed with VideoMach 2.7.2 Software (<http://gromada.com/main/products.php>).

Cilia-driven transport analysis

Transport function of wild type mouse efferent duct cilia ($n=3$) was visualized using particles of $0.5\ \mu\text{m}$ size (FluoSpheres™ Size Kit #1; Thermo Fischer Scientific, Waltham, MA, USA). Videos were recorded with SAVA software (Sisson et al., 2003). All-digital image captures and whole-field analyses of CBF were performed at $\times 40$ magnification with an ES310 Turbo Megaplus High Speed Camera (Kodak, Rochester, NY, USA) connected to an Eclipse Ti Inverted Microscope (Nikon, Tokyo, Japan). Particle transport was analysed by manual tracking using Fiji MTrackJ (Schindelin et al., 2012).

High resolution IF microscopy

Cryosections ($25\ \mu\text{m}$) of male reproductive tracts (testis to vas deferens) from *Mdnah5^{mut/mut}* mice and wild type control siblings (total: $n=6$ *Mdnah5^{wt/wt}*; $n=11$ *Mdnah5^{mut/mut}*; adult male reproductive tract: $n=3/\text{group}$) were collected onto positively charged microscope slides, air-dried and stored at -80°C until use. In addition, we analyzed human sperm cells after ejaculate donation and multiciliated respiratory cells after nasal sampling. Tissue sections were fixed in 4% paraformaldehyde in $\times 1$ PBS (PFA) for 15 min. After permeabilization in PBS including 0.1 Triton X-100 (PBTx), samples were blocked in PBTx/1% bovine serum albumin (BSA) and incubated with primary antibodies overnight at 4°C . Labeling with secondary antibody followed three washing steps with PBTx. Human cell samples were treated, and incubated with primary and secondary antibodies, as reported (Olbrich et al., 2015). Monoclonal mouse anti-acetylated alpha-tubulin antibody (Sigma-Aldrich, Taufkirchen, Germany) was used as a marker for the ciliary or flagellar axoneme. Polyclonal rabbit antibodies directed against DNAH5, DNAI, DNAI2 and GAS8 as well as monoclonal mouse anti-DNAH5 antibody have been reported (Flegauf et al., 2005; Olbrich et al., 2015; Paff et al., 2017). Polyclonal rabbit antibody directed against DNAH8 (HPA028447) was purchased from Sigma Prestige Antibodies (Munich, Germany). Chicken and goat anti-mouse Alexa Fluor 488®, as well as goat anti-rabbit Alexa Fluor 546® (Thermo Fischer Scientific, Waltham, USA) and donkey anti-rabbit Rhodamine Red™-X (Jackson ImmunoResearch Laboratories, West Grove, USA) was used as secondary antibodies. Nuclei were stained with DAPI or Hoechst33342 (Thermo Fischer Scientific, Waltham, USA) and all samples were mounted in fluorescence mounting medium (Dako North America Inc., Carpinteria, USA). IF microscopy images were captured with a Zeiss LSM 880 Confocal Laser Scanning or a Zeiss Apotome Axiovert 200 Microscope (Carl Zeiss Microscopy GmbH, Jena, Germany). Pictures were processed with ZEISS ZEN Imaging Software 2012, AxioVision v.4.8 (Carl Zeiss Microscopy GmbH, Jena, Germany) and Adobe Creative Suite CS5 (Adobe Systems, San José, USA).

Transmission electron microscopy (TEM)

Male reproductive tracts (testis to vas deferens) from *Mdnah5^{wt/wt}* and *Mdnah5^{mut/mut}* males (total: $n=6$ *Mdnah5^{wt/wt}*; $n=11$ *Mdnah5^{mut/mut}*; adult male reproductive tract: $n=3/\text{group}$) were dissected and fixed in 2.5% glutaraldehyde (Sigma-Aldrich, Taufkirchen, Germany). After a pre-fixation for 5 h at 4°C the different regions of interest (testis, efferent ducts, caput, corpus and cauda epididymis and vas deferens) were separated from each other and cut into smaller pieces (size around $2 \times 2\ \text{mm}^2$). Human respiratory cells obtained from nasal brush biopsies and $250\ \mu\text{l}$ of liquefied ejaculates were each suspended in 2.5% glutaraldehyde for fixation. Samples were processed for TEM analysis according to standardized protocols (Wallmeier et al., 2014). Pelleted human cell samples and mouse tissues were contrasted with 1% osmium tetroxide, incubated in a 1, 2-epoxypropan-epon mixture (1:2) at 4°C overnight and finally embedded in epon (SERVA, Heidelberg, Germany). After polymerization, semithin sections were first cut from all samples and stained by toluidine blue. Afterwards, ultrathin sections (80 nm) were prepared and collected onto copper grids for TEM analyses. Samples were analyzed with the transmission electron microscope Philips CM10, and TEM images acquired with a Quemesa camera and the iTEM SIS image acquisition software (both from Olympus Soft Imaging Solutions). Image processing was performed with Adobe Creative Suite CS5. Quantification of sperm in mouse tissue sections from the caput, corpus and cauda epididymis of *Mdnah5^{wt/wt}* and *Mdnah5^{mut/mut}* males, was performed by counting sperm head and flagellar structures in 10 tubule sections per region (total: $n=3$ *Mdnah5^{wt/wt}*; $n=3$ *Mdnah5^{mut/mut}*). Sperm structures within the analyzed epididymal tubule sections were counted using the cell counter plugin from Fiji (Schindelin et al., 2012) and the tubule size measured by square micrometer using the same software.

Statistical analyses

Efferent duct CBF was analysed for statistical significance between distinct samples of *Mdnah5^{mut/mut}* mice and their control siblings ($n=5$ *Mdnah5^{wt/wt}*; $n=7$ *Mdnah5^{mut/mut}* mice) using the two-tailed Student's t-test with Welch's correction for unpaired samples of different variance with GraphPad Prism9 (GraphPad software, La Jolla, CA, USA).

Quantification of sperm in mouse tissue sections from the caput, corpus and cauda epididymis was analysed for statistical significance between *Mdnah5^{wt/wt}* and *Mdnah5^{mut/mut}* mice ($n=3$ *Mdnah5^{wt/wt}*; $n=3$ *Mdnah5^{mut/mut}*) using a Chi-square (χ^2) test with GraphPad Prism9 (GraphPad software, La Jolla, CA, USA).

Hematoxylin and eosin staining of mouse tissues

Cryosections ($10\ \mu\text{m}$) of adult male reproductive tracts (testis to vas deferens) from *Mdnah5^{mut/mut}* mice and wild type control siblings ($n=3/\text{group}$) were fixed in ice-cold (-20°C) methanol and stained using Mayer's hemalum solution and counterstained with a 0.5% alcoholic eosin Y solution (both Merck, Darmstadt, Germany), per manufacturer's protocol. Images were taken with an Eclipse Ti Inverted Microscope and DS-Ri2 camera (Nikon, Tokyo, Japan) and processed using Adobe Creative Suite CS5.

Cultivation of ciliated respiratory epithelial cells

Ciliated respiratory epithelial cells were acquired from the middle turbinate with a nasal brush (Engelbrecht Medicine and Laboratory technology) and resuspended in cell culture medium. Cells were pre-cultured in flasks coated with rat collagen and subsequently processed to air-liquid interface (ALI-) cultures, as previously reported (Hirst *et al.*, 2010; Munye *et al.*, 2016). For the proliferation of cells, PneumaCult™-Ex Medium (Stemcell™) and for the cell differentiation PneumaCult™-ALI Maintenance medium (Stemcell™) supplied with 1% Antibiotic—Antimycotic ×100, were used.

Immunoblotting

Protein extracts were obtained from human control sperm and ciliated respiratory cells cultivated under ALI conditions ($n = 4$ per cell type) by treatment in IGEPAL-Buffer ((50 mM Tris-HCl (pH 8.0), 150 mM NaCl, 1% IGEPAL, 10% Glycerol, 0.5 mM EDTA supplemented with cOmplete™ Mini EDTA-free Protease Inhibitor Cocktail Tablets (Roche) and Phosphatase Inhibitor Cocktail 2 and 3 (Sigma-Aldrich)). Obtained cell lysates were homogenized (2000 rpm, 3 min) using the Mikro-Dismembrator U (Sartorius). A final centrifugation step (12 851 g, 20 min, 4°C) separated extracted proteins from residual cell components. The clarified supernatant was supplemented with loading buffer and reducing agent (10 µl supernatant, 5 µl NuPAGE® 4xLDS sample buffer (novex® by life technologies), 2 µl 1 M DTT, 3 µl distilled water), then heated for 10 min at 70°C. To evaluate the protein content of the final cell lysate, proteins were separated via a NuPAGE® 3%-8% Tris-acetate gel (Invitrogen) and visualized using the Proteo Silver™ Silver Stain kit (Prot-SIL1, Sigma) according to the manufacturer's protocol. For the immunoblotting procedure, protein lysate was separated using a NuPAGE® 3%-8% Tris-acetate gel, then transferred to an Invitrolon™ polyvinylidene difluoride-membrane (novex® by life technologies). Blots were washed twice (5 min each) with Tris-buffered saline plus Tween 20 (TBST) and blocked in 5% BSA in TBST for 4 h at room temperature.

Blots were treated using rabbit polyclonal anti-DNAH5 (Fliegauf *et al.*, 2005) and anti-DNAH8 antibody (HPA028447, Atlas Antibodies) (both diluted 1:1000 in TBST) and horseradish peroxidase-conjugated anti-rabbit antibody (diluted 1:3000; Santa Cruz Biotechnology, Heidelberg, Germany). Blots were developed using ECL Prime Western Blotting Detection Reagent (GE Healthcare Life technologies, Little Chalfont, UK) following manufacturers instructions. Images were taken with the FUSION-SL 3500 WL advanced Imager (VWR International, Erlangen, Germany) and processed using Adobe Creative Suite CS5.

Results

Male reproductive tracts of adult *Mdnah5*^{mut/mut} mice display dilatation of the rete testis and sperm stasis in efferent ducts

Macroscopic examination of male reproductive tracts revealed that, compared to wild type control littermates, *Mdnah5*^{mut/mut} males

display dilatation of the rete testis, visible as a translucent area around the conjunction of the testis to the efferent ducts (Supplementary Fig. S1). Interestingly, a dilatation of the rete testis could already be observed in a prepuberal (Bellve *et al.*, 1977) mutant male (P30) who had not yet completed the first wave of spermatogenesis (Supplementary Fig. S1), (Oakberg, 1956). Histological analyses by hematoxylin-eosin staining confirmed this finding (Fig. 2). Moreover, toluidine blue staining of male reproductive tract semithin sections revealed that sperm cells accumulate in the efferent ducts of adult *Mdnah5* mutant mice, when compared to control littermates (Fig. 2).

We further analyzed this phenotype by TEM in three adult control and mutant mice (P40, P45 and P50). We found that in control littermates the proximal and distal efferent duct regions were largely devoid of sperm, whereas the distal efferent ducts of the corresponding *Mdnah5*^{mut/mut} males contained accumulated sperm (Supplementary Figs. S2–S4). In contrast, the caput, corpus and cauda regions of the control littermate's epididymides harbored a large number of sperm, whereas these regions in the corresponding DNAH5-deficient mice contained either no sperm or a statistically significant reduced number of sperm (Supplementary Figs S5–S7 and Supplementary Table SII). Quantification of sperm head and flagellar structures in control epididymal sections revealed an average number of 338, 184 and 131 sperm cells per 1000 µm² tubule in the caput, corpus and cauda regions, respectively. In contrast, the P40 *Mdnah5*^{mut/mut} male showed a reduction in sperm count of 98–100% in all three epididymal regions (Supplementary Fig. S5, Supplementary Fig. S8 and Supplementary Table SII) and the P50 *Mdnah5*^{mut/mut} male showed a reduction of 60% in the caput and 99–100% in the corpus and cauda epididymis (Supplementary Figs S7–S8 and Supplementary Table SII). Surprisingly, the P45 *Mdnah5*^{mut/mut} male had many more spermatozoa along the epididymis compared to the P40 and P50 mutant males. However, quantification analysis showed that the sperm quantity was lower by 70% in the epididymal head, 60% in the epididymal corpus, and 79% in the epididymal cauda region compared to the control littermate (Supplementary Fig. S6, Supplementary Fig. S8 and Supplementary Table SII).

Altogether, these findings indicate that *Mdnah5*^{mut/mut} males can exhibit an obstructive sperm stasis in the efferent duct tubule system.

Efferent duct cilia of *Mdnah5*^{mut/mut} mice display ODA defects, whereas sperm flagella present a normal ultrastructure with ODAs

We next investigated whether DNAH5 deficiency affected the ultrastructure of efferent duct cilia and/or sperm flagella in mice. Using TEM to investigate general ODA structure in *Mdnah5*^{mut/mut} mice, we observed axonemal ODA defects in efferent duct cilia but not in sperm flagella (Fig. 3A–D, Supplementary Fig. S9). Then, we examined the presence of DNAH5 in both control and *Mdnah5*^{mut/mut} mice: using anti-DNAH5 antibodies (Fliegauf *et al.*, 2005) and IF, we detected panaxonemal localization of DNAH5 (Fig. 3E, upper panel) in efferent duct cilia of control mice but not *Mdnah5*^{mut/mut} mice (Fig. 3E, lower panel). Interestingly, DNAH5 was not detectable in the sperm flagella in both adult wild type control and *Mdnah5*^{mut/mut} male mice (Fig. 3F).

We also used IF to examine the localization of other known ODA components, the dynein intermediate chains DNAIL1 (Pennarun *et al.*,

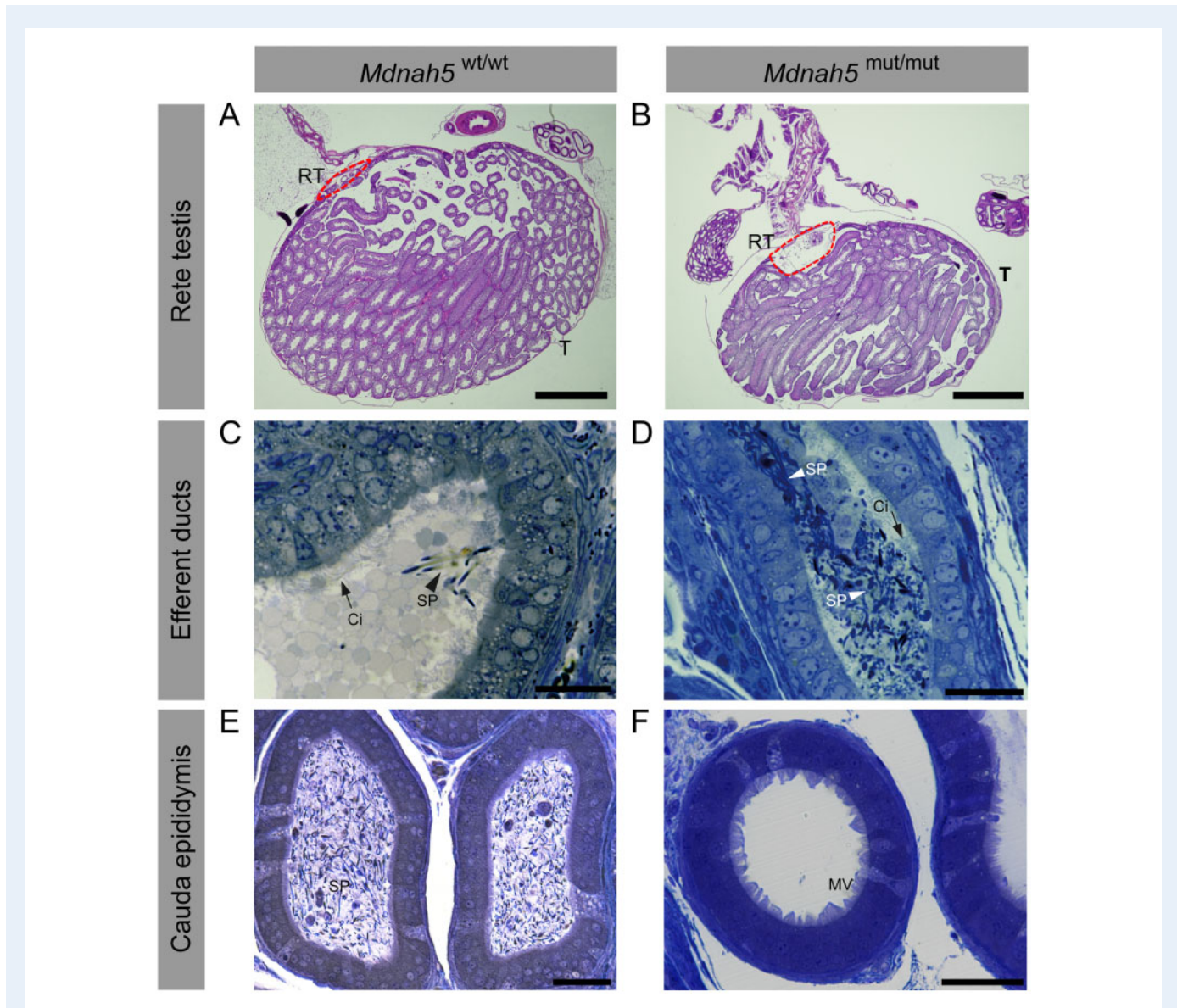


Figure 2. Adult *Mdnah5* homozygous mutant male mice display enlargement of the rete testes and sperm accumulation in the efferent duct tract. **A** and **B**, hematoxylin and eosin staining of (A) control and (B) *Mdnah5*^{mut/mut} testes (T) show that compared to control littermates, *Mdnah5*^{mut/mut} males present a dilatation of the rete testes (RT, red line). **C–F**, toluidine blue staining of efferent duct and cauda epididymis semi thin sections. **C** and **D**, cilia (Ci) line efferent duct lumen of control (*Mdnah5*^{wt/wt}) and *Mdnah5*^{mut/mut} mice. Controls present few isolated spermatozoa (SP). Sperm accumulation is clearly visualized in the *Mdnah5*^{mut/mut} mouse. **E** and **F**, opposite distribution of spermatozoa is observed within the cauda epididymis: a large amount of spermatozoa is present in the control but only few are visible in the *Mdnah5*^{mut/mut} male. One example is representatively shown for a biological replicate of three adult mice ($n=3$). Scale bars represent 1000 μm (A, B), 50 μm (C–F). MV: microvilli.

2002; Paff et al., 2017) and DNAI2 (Loges et al., 2008; Paff et al., 2017), in control and *Mdnah5*^{mut/mut} mice. Both proteins were detectable in the control mice's efferent duct cilia, but neither were present in the *Mdnah5*^{mut/mut} mice's efferent duct cilia (Fig. 3G and I). However, DNAI1 and DNAI2 displayed panaxonemal localization in both the adult wild type control and the *Mdnah5*^{mut/mut} male mice's sperm flagella (Fig. 3H and J).

These findings demonstrate that *Mdnah5*^{mut/mut} mice specifically lost ODAs in their efferent duct cilia, similar to respiratory cilia (Nöthe-Menchen et al., 2019), but not in their sperm flagella and provide

evidence for a conserved function of DNAH5 in cell types with multiple motile cilia but not sperm flagella.

ODA defects in efferent duct cilia of *Mdnah5*^{mut/mut} mice cause ciliary dysmotility, whereas DNAH5 deficiency does not affect sperm flagellar motility

To determine whether loss of ODAs in the efferent duct cilia of *Mdnah5*^{mut/mut} mice results in ciliary dysmotility and represents the

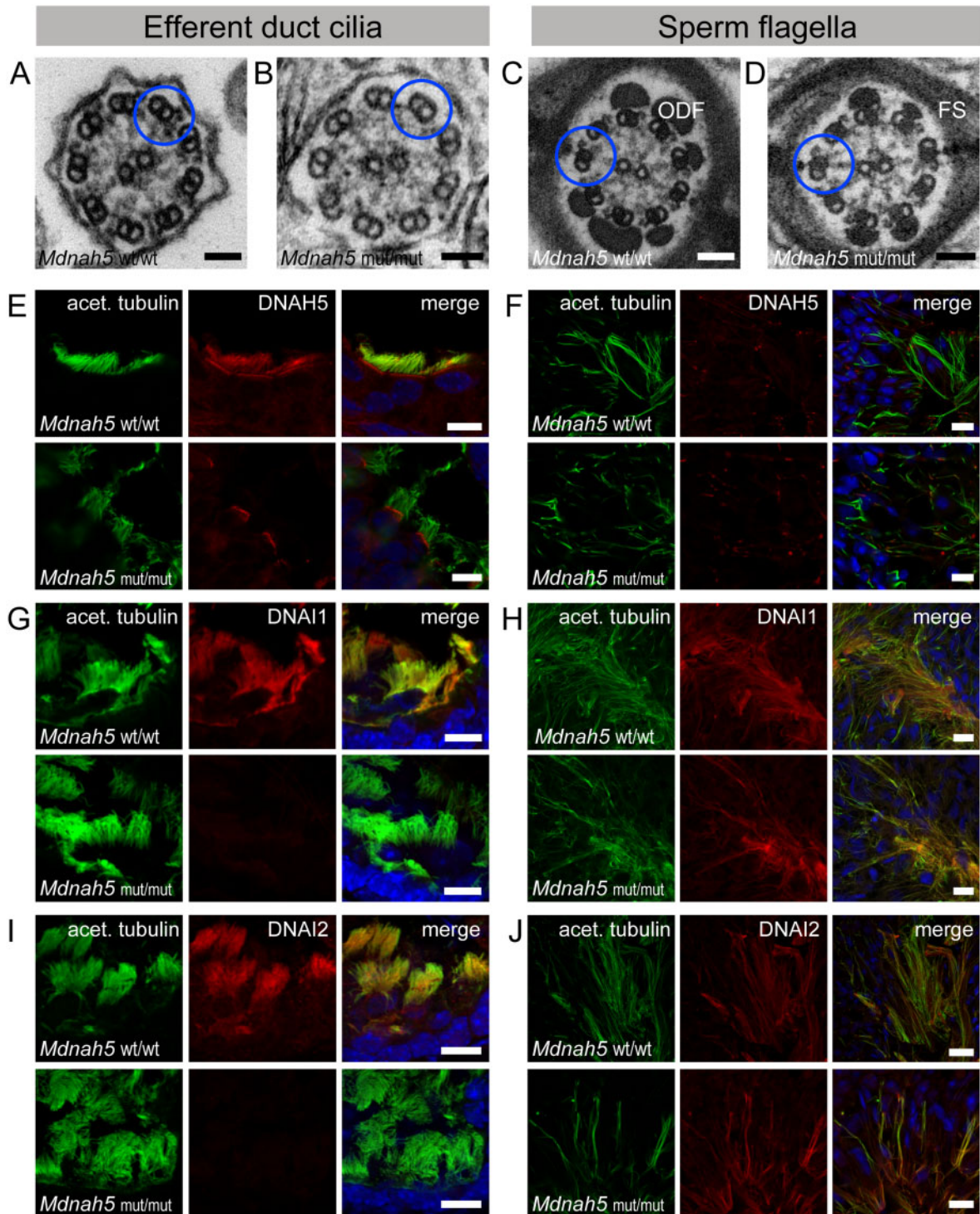


Figure 3. *Mdnah5* homozygous mutant male mice show loss of ODAs in efferent duct cilia but not sperm flagella. **A**, TEM of control (*Mdnah5*^{wt/wt}) efferent duct cilia. **B**, absence of ODAs in mutant (*Mdnah5*^{mut/mut}) efferent duct cilia; ODA presence in **(C)** control and **(D)** mutant sperm flagella. **E**, IF co-staining confirms DNAH5 (red) presence in control efferent duct cilia along the entire ciliary length marked with an antibody against acetylated alpha-tubulin (green) and DNAH5 loss in *Mdnah5*-mutant tissue. **F**, IF staining on testicular sections show that DNAH5 (red) is not present in control and *Mdnah5*-mutant mouse sperm flagella. **G**, DNAI1 (red) localizes to control efferent duct cilia, but not in *Mdnah5*^{mut/mut} mice. **H**, IF staining on testicular sections show that DNAI1 (red) localizes to sperm flagella in control and *Mdnah5*^{mut/mut} male. **I**, as for the other ODA components, also DNAI2 (red) localizes to control efferent duct cilia, but not in *Mdnah5*^{mut/mut} mice. **J**, IF staining on testicular sections show that control sperm cells (upper panel) and those of the *Mdnah5*-mutant male (lower panel), display both panaxonemal localization for DNAI2 (depicted in red). Biological replicate for efferent duct cilia: *n* = 9 control mice; *n* = 11 *Mdnah5* homozygous mutant mice. Biological replicate for sperm flagella: *n* = 3/group. Nuclei (blue) were stained with DAPI. Scale bars represent 50 nm (A–D), 10 μm (E–J).

underlying cause of their obstructive sperm stasis, we first analyzed efferent duct cilia in control mice in more detail. By TEM we found that efferent duct cilia display regularly disposed basal foot processes and oriented central pair complexes (Fig. 4A and B), which is consistent with the directed transport function of multiple motile cilia in other tissues (Fliegauf et al., 2007). Thus, these findings suggest that efferent duct cilia have inherent polarity and a coordinated and planar beat pattern, similar to multiple motile respiratory cilia (Mitchell et al., 2007). To scrutinize this hypothesis, we performed HVMA. Efferent duct cilia display a median CBF of 13 Hz at 37°C. The ciliary beat pattern comprises effective forward and backward recovery strokes, resembling the beat pattern of respiratory cilia and suggesting a directed transport

function for efferent duct cilia (Supplementary Videos S1 and S2). We confirmed this by visualizing the transport of plastic beads (0.5 µm diameter) applied to the efferent duct samples, showing a median transport velocity of 130 µm/s (Fig. 4C and D).

As reported for other types of DNAH5 deficient motile cilia (Ibanez-Tallon, 2002; Fliegauf et al., 2005; Nöthe-Menchen et al., 2019), the DNAH5-deficient efferent duct cilia were—compared to controls—mostly immotile, with some cilia displaying residual flickering motility (Supplementary Videos S3 and S4). At 37°C, the median CBF was significantly reduced from 13 Hz (controls) to 3 Hz (*Mdnah5^{mut/mut}*) ($P < 0.0001$; ***, Fig. 5 and Supplementary Table SIII).

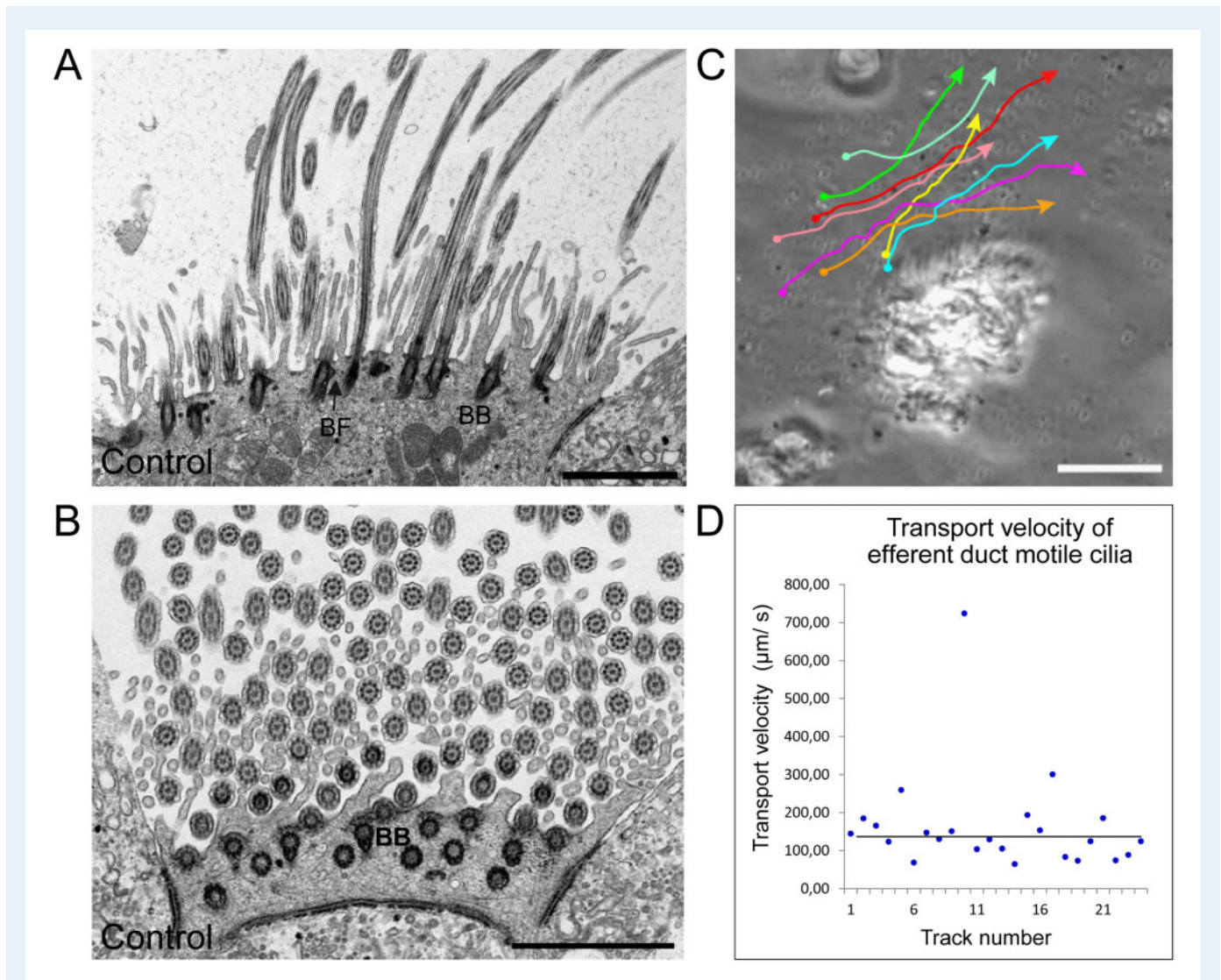


Figure 4. Mouse efferent duct cilia display a regular orientation and directed beating pattern. **A** and **B**, TEM analysis of ciliary cross sections in control mouse efferent ducts. **A**, longitudinal sections of efferent duct cilia displaying regular disposed basal bodies and basal foot processes. **B**, central pairs of efferent duct cilia (Ci) are oriented in a regular fashion as indicated by the red bars. **C**, manual tracking of 0.5 µm plastic beads applied on efferent duct cilia confirms that this cilia type displays a directed beating pattern. **D**, evaluation of the transport velocity of control efferent duct cilia shows that applied beads are mobilized with a median velocity of 130 µm/s. Biological replicate: $n=3$; Scale bars represent 2 µm (A and B), 50 µm (C).

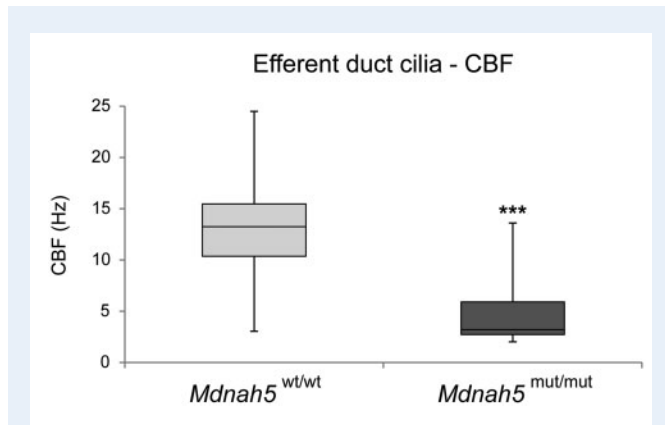


Figure 5. CBF of efferent duct cilia is significantly reduced in *Mdnah5* homozygous mutant male mice. Compared to control mice (*Mdnah5*^{wt/wt}), statistical analysis by unpaired two-tailed student's *t*-test with Welch's correction reveals a significant reduction of CBF (in Hz: Hertz) of motile efferent duct cilia in *Mdnah5*^{mut/mut} mice. Biological replicate: *n*=5 control group; *n*=7 *Mdnah5* homozygous mutant mice, *P*<0.001: ***.

By contrast, the motility of sperm cells isolated from the epididymal body of P45 and P50 control and *Mdnah5*^{mut/mut} male mice was comparable, confirming that DNAH5 deficiency does not affect sperm flagella motility (Supplementary Videos S5 and S6).

Overall, these results confirm that the movement of efferent duct cilia in *Mdnah5*^{mut/mut} male mice is impaired, but that their sperm flagella are normal. As such, sperm flow obstruction and reduction of sperm number in the reproductive tracts of the *Mdnah5*^{mut/mut} male is solely caused by impaired motility of efferent duct cilia.

DNAH5 deficient men with PCD can display severely reduced sperm numbers and dilatation of the epididymal head

To address whether the disease mechanism identified in *Mdnah5*^{mut/mut} mice is conserved in the human male reproductive system, we analyzed the fertility status of four young males with ages spanning from 19 to 29 years, carrying bi-allelic DNAH5 loss-of-function mutations: siblings OP-116 III and II2 (Exon 20: c.3037_3040delAGCG, p. V1014Lfs*20 het. + Exon 25: c.3949C>T, p. Q1317* het.), OP-399 III (Exon 38: c.6343delA, p. I2115* het. + Exon 76: c.13194_13197delCAGA, p. D4398Efs*16 het.), (Wallmeier, 2012), and OP-1781 III (Exon 51: c.8497C>T, p. R2833C het. (PolyPhen-2 prediction score: 1.00; probably damaging, (Adzhubei et al., 2010)) + Exon 63: c.10815delT, p. P3606Hfs*23 het.), (Supplementary Fig. S10).

Initial semen analysis of all four DNAH5-mutant human males revealed severe oligozoospermia (<4 million sperm/ml of ejaculate) with preserved progressive motility of sperm cells in OP-116 III, OP-116 II2 and OP-399 III; OP-1781 III suffered from azoospermia, i.e. no sperm in the ejaculate. In three of these individuals (OP-116 III, OP-399 III and OP-1781 III) a second semen analysis was performed, and OP-116 III and OP-1781 III also underwent an andrologic examination. The second semen analysis yielded normal sperm numbers (normozoospermia) in the ejaculate of OP-116 III, whereas

OP-399 III displayed azoospermia, and azoospermia was confirmed in OP-1781 III (Supplementary Table SIV).

Sonographic examination of the testis and epididymis in DNAH5-mutant individuals OP-116 III and OP-1781 III revealed a bilateral enlargement of the caput epididymis (Fig. 6) when compared to a healthy control individual and to published maximum reference values of epididymal head height (Pilatz et al., 2013). Consistent with the phenotype observed in *Mdnah5*^{mut/mut} mice, these findings indicate an obstructive sperm stasis, presumably due to dysfunction of efferent duct cilia motility.

Sperm of DNAH5 mutated male individuals with PCD present a regular ultrastructure with ODAs and normal motility

To assess the motility and structure of sperm of individuals OP-116 III and OP-116 II2, we performed HVMA and TEM. The beating pattern (Supplementary Videos S7–S9) and ultrastructure (i.e. clearly visible ODAs) of their sperm flagella was similar to sperm flagella from healthy donors (Fig. 7A–H), confirming normal ODA composition of DNAH5 mutant sperm flagella.

To further refine the structure of sperm flagella of OP-116 III, OP-116 II2 and OP-399 III, we performed IF on sperm flagella compared to respiratory epithelial cells using antibodies targeting ODA components in motile cilia. We confirmed ODA defects in multiciliated respiratory epithelial cells of all analyzed DNAH5-mutant individuals; the loss of ODAs from the ciliary axonemes was demonstrated by TEM, and absence of the ODA proteins DNAH5 and the ODA intermediate chain components DNAI1 and DNAI2 in cilia were confirmed by IF (Supplementary Figs S11 and S12 and Supplementary Table SV).

As observed in mice, DNAH5 was undetectable in sperm flagella of healthy controls and DNAH5-mutants OP-116 III, OP-116 II2 (Fig. 7I–K) and OP-399 III (Supplementary Fig. S13). Consistently, DNAI1 and DNAI2 displayed the expected panaxonemal localization in all control- and DNAH5-mutant sperm flagella of individuals OP-116 III and OP-116 II2 (Fig. 7L–N). Thus, DNAH5 displays an evolutionarily conserved functional role for ODA composition in multiple motile cilia, but not in sperm flagella.

To complete our analysis and to clarify which paralogous protein might substitute the functional role of DNAH5 in sperm flagella, we performed western blot and IF analyses using antibodies directed against DNAH8, like DNAH5 an ortholog to the ODA γ -heavy chain of the biflagellated alga *Chlamydomonas reinhardtii* (Pazour et al., 2006). DNAH8 was lacking in respiratory epithelial cilia (data not shown) but localized panaxonemal to the sperm flagella of healthy controls and DNAH5-mutant individuals (Fig. 8 and Supplementary Fig. S14).

Discussion

We report findings that support a novel disease mechanism for male oligozoospermia: our data demonstrate that loss of DNAH5 can lead to obstructive oligozoospermia-associated male infertility caused by dysfunction of efferent duct motile cilia, without affecting sperm flagella structure and function.

It is currently proposed that efferent ducts facilitate sperm transport to the epididymis by performing several functions. These include

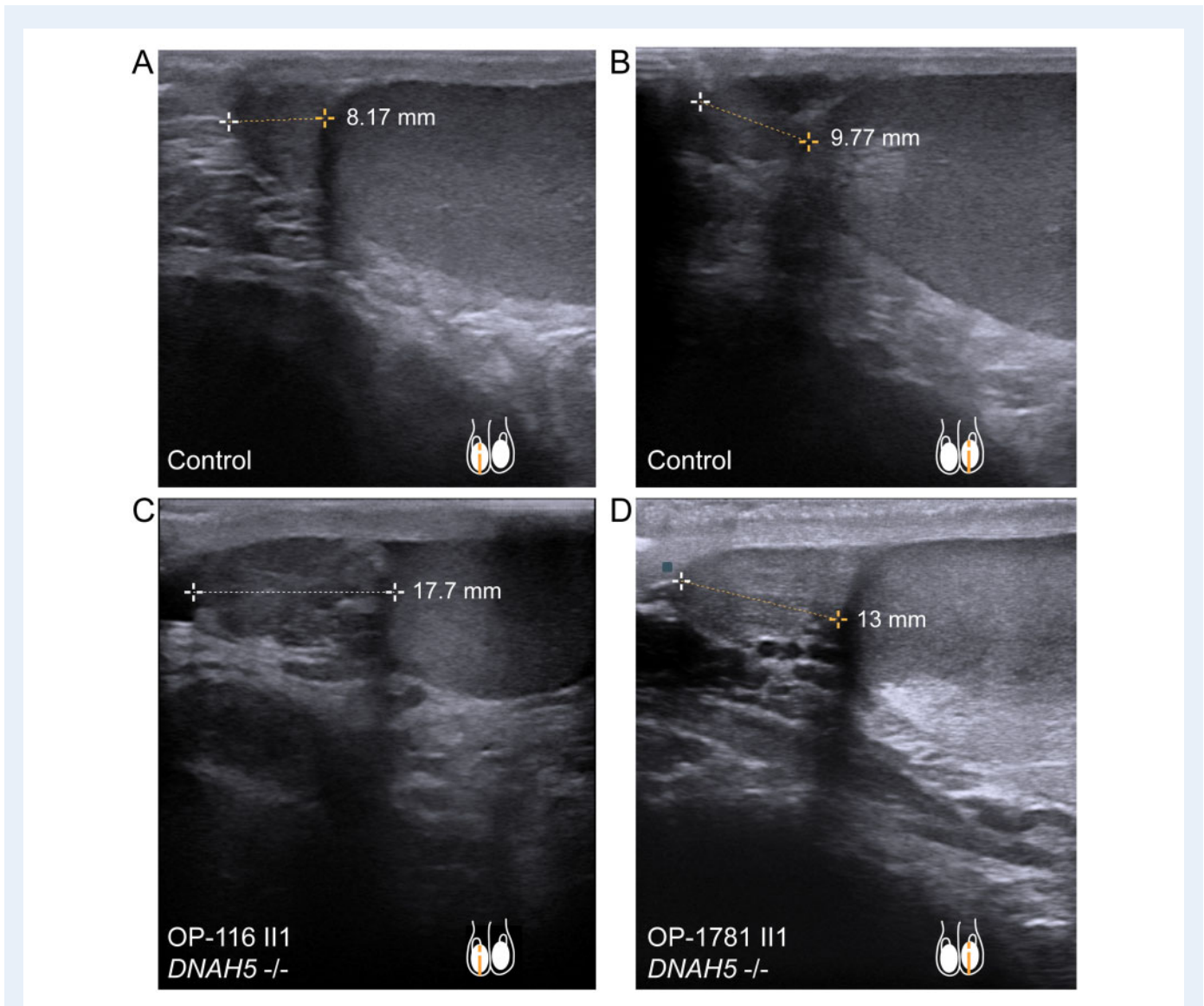


Figure 6. DNAH5-mutant male individuals present enlargement of the epididymal head. **A** and **B**, sonographs of respectively right (A) and left (B) testis and epididymal head, in a healthy control individual. Epididymal head height measures 8.17 mm (A) and 9.77 mm (B). **C**, individual OP-116 III and **D**, individual OP-1781 III, carrying disease causing mutations in *DNAH5*, present an epididymal head height of 17.7 mm (OP-116 III) and 13 mm (OP-1781 III), respectively. This indicates an enlargement of the epididymal head size, compared to control (A, B) and published maximum reference values of 11.6 mm (right epididymal head) and 11.3 mm (left epididymal head) (Pilatz et al., 2013).

secretion and absorption of fluid via the seminiferous epithelium, contraction of the tubular myoepithelial layer, vacuum generation following ejaculation, and increment of pressure caused by the branching and convergence of efferent ducts (Hess, 2014). While it was initially assumed that efferent duct cilia transport sperm cells to the epididymis, recent studies suggest that the smooth muscle contraction of the efferent ducts move sperm cells outwards, while motile cilia create, with their beating, a swirling motion of the seminiferous fluid, keeping sperm cells in suspension and avoiding them from clogging (Yuan et al., 2019).

Similar to our findings in *Mdnah5*^{mut/mut} male mice, recent studies have demonstrated that mice deficient for factors necessary for the

ciliogenesis of multiple motile cilia, such as the Mir449/34 family of miRNAs, the *E2f* transcription factors, or the Geminin family members GEMC1 and MCIDAS, as well as the atypical cyclin CCNO, display obstructive oligozoospermia and infertility (Danielian et al., 2016; Terré et al., 2019; Yuan et al., 2019). In all of the mouse models mentioned above, the ciliogenesis defect (reduced number of multiple motile cilia) may also affect non-motility related ciliary functions such as chemosensing (Shah et al., 2009). By contrast, our *Mdnah5*^{mut/mut} mice do not show any ciliogenesis defect, and they lack no other ciliary component than the motor unit ODA. Therefore, we conclude that even in the absence of other disease mechanisms (e.g. abnormal

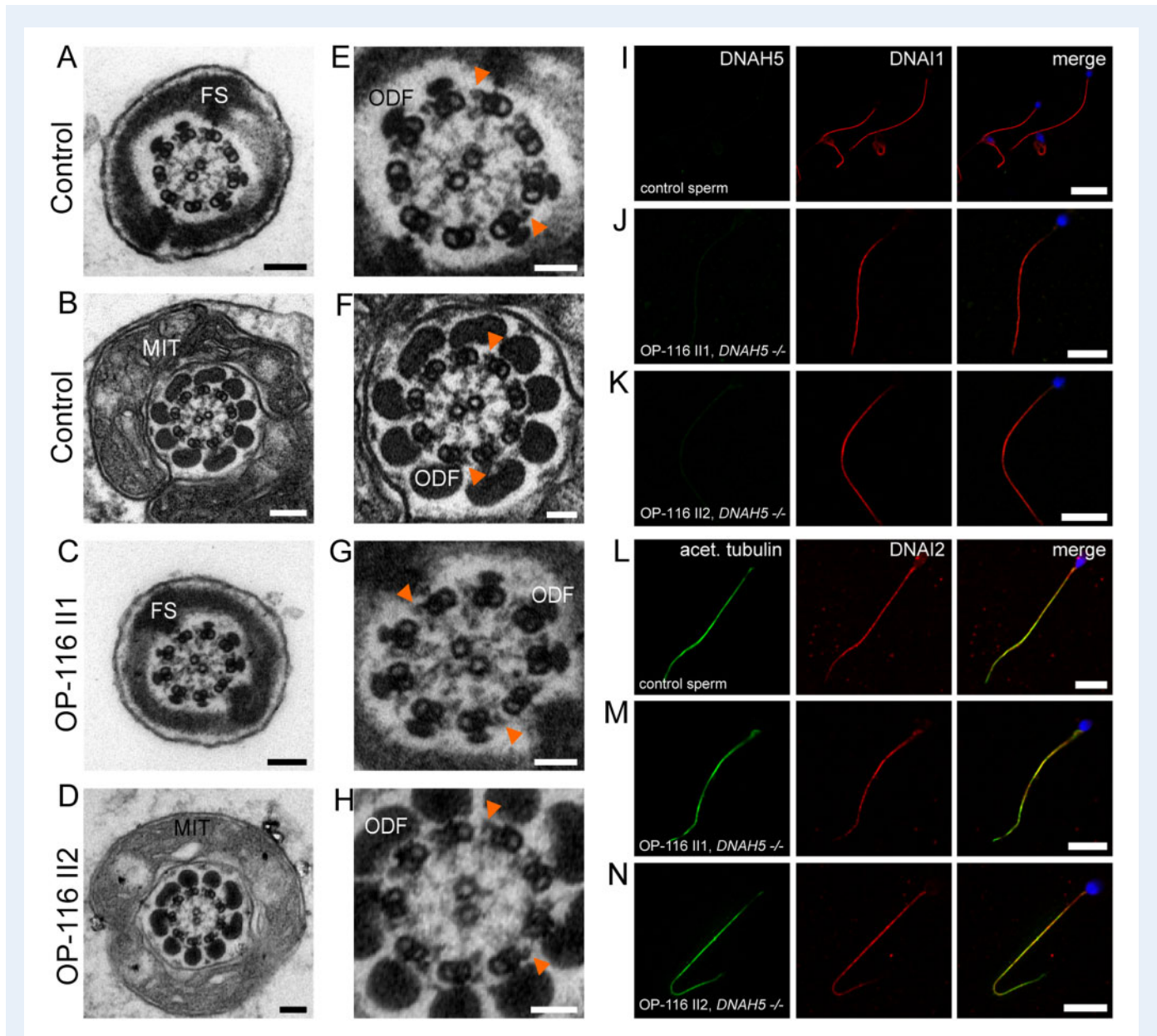


Figure 7. ODA protein DNAH5 is not present in human sperm flagella. **A** and **B**, TEM of control sperm cells showing the 9 + 2 axoneme with clearly visible ODAs and accessory structures (FS: fibrous sheath, MIT: mitochondria, and ODF: outer dense fibers). **C** and **D**, DNAH5 deficiency does not cause ODA defects of sperm flagellar axonemes. **E–H**, magnifications of **A–D**, orange arrowheads exemplarily indicate ODAs. **I, J, K, L**, IF co-staining assessing DNAH5 absence and panaxonemal localization of DNAI1 in human control and DNAH5-deficient sperm cells. **L**, control sperm cells display a panaxonemal flagellar localization of DNAI2 (red) that co-localizes (yellow in the merged image) with the flagellar marker acetylated alpha-tubulin (depicted in green). **M** and **N**, sperm flagella of individuals with PCD causing compound heterozygous mutations in *DNAH5* display an unaltered localization pattern of DNAI2, indicating that DNAH5 is not a component of the ODA in sperm flagella. Nuclei (blue) were stained with DAPI. Scale bars represent 100 nm (A–D), 50 nm (E–H), 10 μm (I–N).

chemosensing of cilia), the loss of ciliary motility within efferent ducts is sufficient to cause obstructive oligozoospermia in mice.

However, the animal model used in our study presents limitations that require further discussion. The sensitivity of *Mdnah5*^{mut/mut} mice to the postnatal formation of hydrocephalus restricts the number of animals surviving until adulthood and thus reduces availability of those mutants for more detailed fertility analyses, and renders mating

experiments impossible. Nonetheless, we show equivalent data in human DNAH5-deficient male individuals where severely reduced sperm counts and dilatations of the epididymal head size, but normal sperm motility, are observed. This is consistent with the phenotype observed in the male reproductive tracts of *Mdnah5*^{mut/mut} mice, further corroborating our findings.

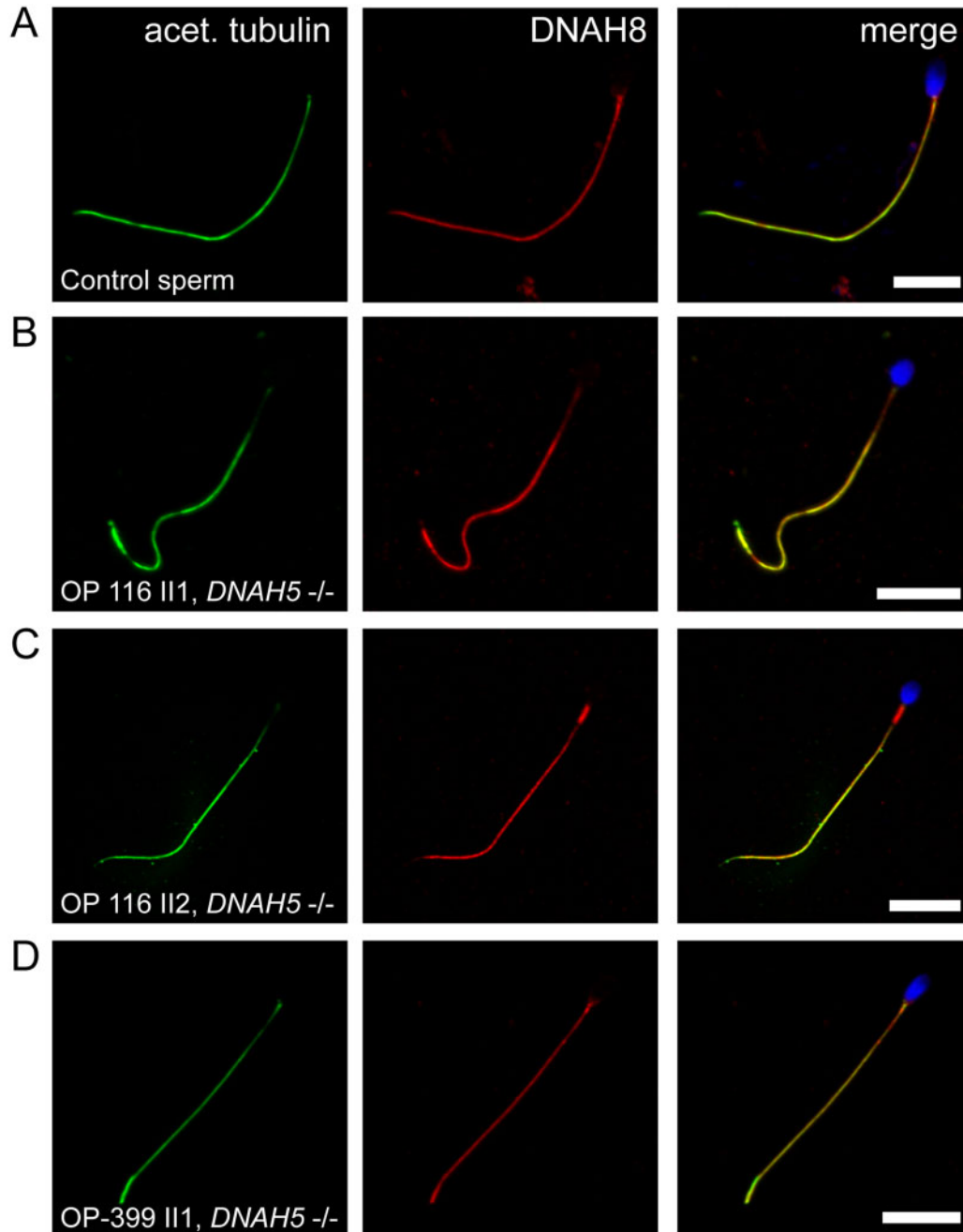


Figure 8. DNAH8 is present in sperm flagella of DNAH5-deficient individuals. **A**, IF analysis showing DNAH8 panaxonal localization in human control sperm cells. **B–D**, same staining procedure shows that sperm flagella of *DNAH5*-mutant individuals present an unaltered DNAH8 localization along the entire flagellar length. This is consistent with the observed unaltered sperm ultrastructure of *DNAH5*-deficient individuals and the hypothesis that DNAH8, as a paralogue of DNAH5, developed a specific function in sperm flagella. Flagellar marker: acet. tubulin (acetylated alpha-tubulin). Nuclei (blue) were stained with DAPI. Scale bars represent 10 μ m.

Interestingly, a second semen analysis in a *DNAH5*-deficient male studied here showed parameters consistent with normal sperm function (normozoospermia). Unfortunately, all human study participants are of a young age and not yet interested in fatherhood, so information on the ability to father a child naturally with their partner is

lacking: but natural fatherhood in PCD patients with isolated ODA defects in respiratory cilia, including *DNAH5*-deficient individuals, is reported and also observed more frequently than in PCD patients with defects of other categories, such as combined outer and inner dynein arm defects (Vanaken et al., 2017; Sironen et al., 2019). Similarly,

we observed a smaller reduction in sperm count in the epididymis (60–79%) of the P45 *Mdnah5* mutant mouse, compared with the other *Mdnah5* mutant mice (P40 and P50) analyzed in this study, which have almost no sperm along the epididymis (reduction of sperm count up to 98–100%). This suggests that the sperm obstruction along the male reproductive tract is less pronounced in the P45 mutant *Mdnah5* mouse. The current model proposes that ciliary motility within the efferent ducts supports but is not the exclusive key driver for the passage of sperm to the epididymis (Hess, 2014; Yuan *et al.*, 2019). It can therefore be assumed that dysmotility of the efferent duct cilia alone is a cause of obstructive oligozoospermia, albeit with some phenotypic variability, since other factors, such as tubular myoepithelial contraction and vacuum generation after ejaculation, also facilitate sperm passage toward the epididymis (Hess, 2014).

Previously, we reported of two infertile DNAH5-deficient males with low sperm counts or azoospermia (Fliegauf *et al.*, 2005). However, motile sperm cells were not observed in the semen analysis of the DNAH5-deficient male with low sperm counts. Moreover, by using a polyclonal antibody we previously localized DNAH5 in the proximal flagellar axoneme in both human control and *DNAH5* mutant sperm flagella (Fliegauf *et al.*, 2005). Nevertheless, potential limitations of this polyclonal antibody were also mentioned in that study because it also targeted proteins from the microtubule organizing centers. Here, we show that DNAH5-deficient men present progressive motile sperm levels above the lowest WHO reference value (Supplementary Table SIV) and that DNAH5 is not localized in sperm flagella, as demonstrated by IF analysis (Fig. 7I–N and Supplementary Fig. S13). This clearly indicates that DNAH5 is not a sperm flagellar component. In addition, our data highlight recent findings on the presence of tissue-specific paralogs of ODA heavy chains. Thus, DNAH9, DNAH11 (orthologues to the β -heavy chain in the green algae *C. reinhardtii*), and DNAH5 (ortholog to the γ -heavy chain in the green algae *C. reinhardtii*) are found in respiratory cilia, whereas ODAs in sperm flagella contain DNAH17 (ortholog to β -heavy chain) and DNAH8 (ortholog to γ -heavy chain), (Fliegauf *et al.*, 2005; Whitfield *et al.*, 2019): the latter represents the sperm-specific paralog to DNAH5 and is associated with male infertility by causing sperm immotility and multiple morphological abnormalities (Whitfield *et al.*, 2019; Liu *et al.*, 2020). Our findings showing DNAH8 localization in sperm flagella of healthy control and *DNAH5*-mutant individuals are consistent with data published by Whitfield *et al.* (2019) and corroborate our assumption that DNAH5 and DNAH8 have diverged from the ancestral ODA- γ -heavy chain gene (Kollmar, 2016) and that DNAH8 but not DNAH5 is relevant in sperm flagella (Samant *et al.*, 2002), consistent with normal sperm flagella in *DNAH5*-mutant individuals.

In conclusion, we propose that ciliary beating of the efferent duct epithelium is essential for the passage of sperm along the male reproductive system, and loss of this motility in efferent ducts is sufficient to cause oligozoospermia in mice and most likely in men. This novel mechanism causing oligozoospermia is distinct from sperm flagellar dysmotility (asthenozoospermia) and expands the disease spectrum of motile ciliopathies.

Our findings will impact infertility research, especially research on idiopathic cases of male infertility represented by oligozoospermia and asthenozoospermia (Bracke *et al.*, 2018). Our work suggests that research in idiopathic oligozoospermia should now also include the role of efferent duct cilia dysmotility. Since several drugs, such as beta

blockers, have been shown to result in reduced CBF of respiratory cells (Workman and Cohen, 2014), such medications might also affect efferent duct cilia motility, potentially explaining relevant side effects like oligozoospermia. Thus, the identification of environmental factors as well as other genetic defects responsible for efferent duct cilia dysfunction will improve the understanding of oligozoospermia and idiopathic male infertility.

Data availability

All data supporting this study are available in the main text and in the [Supplementary Information](#).

Acknowledgements

The authors thank the individuals with PCD and their families for participating in this study and acknowledge the German patient support group 'Kartagener Syndrom und Primaere Ciliaere Dyskinesie e. V.'. For the excellent technical assistance, the authors thank M. Herting, D. Ernst, L. Schwiddessen, A. Dorßen, K. Wohlgemuth, A. Borgscheiper, A. C. Robbers, S. Sivalingam and the technicians from the andrology laboratory at the Center for Reproductive Medicine and Andrology (CeRA), University Clinics, Münster (Germany). For the excellent care of study animals, the authors thank F. J. Seesing. For the excellent organizational assistance during the study, the authors thank the study nurses S. Helms and M. Tekaas. We thank Dr Celeste Brenneka for language editing of the manuscript. Several authors of this study are healthcare professionals in the European Reference Networks ERN-LUNG and/or Endo-ERN.

Authors' roles

P.P and H. Omran designed and directed the project. I.A. and T.N M. conducted the overall study and performed all mouse analyses presented in this study. I.A. performed IF analyses on human sperm and respiratory cells obtained from participating individuals. Furthermore, I.A. executed immunoblot analyses under the supervision of G.W.D. and N.T.L. and together with H. Olbrich mutational analyses. A.C.R. processed, embedded and cut all fixed cell samples and mouse tissues for TEM analyses. J.R. and T.K. recruited healthy subjects for sampling control ejaculates and performed nasal brush biopsies in these individuals. H. Omran, J.R. and T.K. recruited the affected individuals that participated in this study and visited them together with J.W., providing clinical samples and data. S.K. and T.S. collaborated in this study with clinical data on the fertility status of participating individuals and providing access to their laboratories for semen analyses. I.A., T.N.M., P.P. and H. Omran interpreted the data and wrote the manuscript. N.T.L., G.W.D., J.R., T.K., J.W., H. Olbrich., S.K. and T.S. commented on the manuscript.

Funding

This work was supported by grants from the Deutsche Forschungsgemeinschaft (DFG, OM6/4, OM6/7, OM6/8, OM6/10,

DFG CRU 326(subproject OM6/11-2 (H.Omran), RA3522/1-1 (J.R.)), WA4283/1-1 (J.W.), OL450/1 (H.Olbrich) and HJ7/1-1 (R.H.)), the Interdisziplinäres Zentrum für Klinische Forschung Muenster (Om2/009/12 and Om2/015/16), the European Commission (BESTCILIA, EU FP7, Grant agreement (GA) 305404; LYSOCIL (Horizon2020 GA 811087), Registry Warehouse (Horizon2020 GA 777295)), COST action BEAT-PCD, the Schroeder Stiftung, Kindness for Kids (H. Omran), Eva Luise und Horst Köhler Stiftung and Care-for Rare Foundation.

Conflict of interest

The authors declare no competing financial interests.

References

- Adzhubei IA, Schmidt S, Peshkin L, Ramensky VE, Gerasimova A, Bork P, Kondrashov AS, Sunyaev SR. A method and server for predicting damaging missense mutations. *Nat Methods* 2010;**7**: 248–249.
- Becker O. Ueber Flimmerepithelium im Nebenhoden des Menschen. *Wiener Medizinische Wochenschrift* 1856;**6**:184.
- Bellve AR, Cavicchia JC, Millette CF, O'Brien DA, Bhatnagar YM, Dym M. Spermatogenic cells of the prepuberal mouse. Isolation and morphological characterization. *J Cell Biol* 1977;**74**:68–85.
- Björndahl L, Barratt CLR, Mortimer D, Jouannet P. 'How to count sperm properly': checklist for acceptability of studies based on human semen analysis. *Hum Reprod* 2016;**31**:227–232.
- Bracke A, Peeters K, Punjabi U, Hoogewijs D, Dewilde S. A search for molecular mechanisms underlying male idiopathic infertility. *Reprod Biomed Online* 2018;**36**:327–339.
- Danielian PS, Hess RA, Lees JA. E2f4 and E2f5 are essential for the development of the male reproductive system. *Cell Cycle* 2016;**15**: 250–260.
- Erdfelder E, FAul F, Buchner A, Lang AG. Statistical power analyses using GPower 3.1: Tests for correlation and regression analyses. *Behav Res Methods* 2009;**41**:1149–1160.
- Faul F, Erdfelder E, Lang AG, Buchner AG. Power 3: A flexible statistical power analysis program for the social, behavioral, and biomedical sciences. *Behav Res Methods* 2007;**39**:175–191.
- Fliegauf M, Benzing T, Omran H. When cilia go bad: Cilia defects and ciliopathies. *Nat Rev Mol Cell Biol* 2007;**8**:880–893.
- Fliegauf M, Olbrich H, Horvath J, Wildhaber JH, Zariwala MA, Kennedy M, Knowles MR, Omran H. Mislocalization of DNAH5 and DNAH9 in respiratory cells from patients with primary ciliary dyskinesia. *Am J Respir Crit Care Med* 2005;**171**:1343–1349.
- Hess RA. The efferent ductules: Structure and functions. In: B Robaire, BT Hinton (eds). *The Epididymis: From Molecules to Clinical Practice*. Boston, MA: Springer, 2002,49–80.
- Hess RA. Disruption of estrogen receptor signaling and similar pathways in the efferent ductules and initial segment of the epididymis. *Spermatogenesis* 2014;**4**:e979103.
- Hess RA, Bunick D, Lee KH, Bahr J, Taylor JA, Korach KS, Lubahn DB. A role for oestrogens in the male reproductive system. *Nature* 1997;**390**:509–512.
- Hirst RA, Rutman A, Williams G, O'Callaghan C. Ciliated air-liquid cultures as an aid to diagnostic testing of primary ciliary dyskinesia. *Chest* 2010;**138**:1441–1447.
- Höben IM, Hjejji R, Olbrich H, Dougherty GW, Nöthe-Menchen T, Aprea I, Frank D, Pennekamp P, Dworniczak B, Wallmeier J et al. Mutations in C11orf70 cause primary ciliary dyskinesia with randomization of left/right body asymmetry due to defects of outer and inner dynein arms. *Am J Hum Genet* 2018;**102**:973–984.
- Hornef N, Olbrich H, Horvath J, Zariwala MA, Fliegauf M, Loges NT, Wildhaber J, Noone PG, Kennedy M, Antonarakis SE et al. DNAH5 mutations are a common cause of primary ciliary dyskinesia with outer dynein arm defects. *Am J Respir Crit Care Med* 2006;**174**:120–126.
- Ibanez-Tallon I. Loss of function of axonemal dynein Mdnah5 causes primary ciliary dyskinesia and hydrocephalus. *Hum Mol Genet* 2002;**11**:715–721.
- Ibañez-Tallon I, Pagenstecher A, Fliegauf M, Olbrich H, Kispert A, Ketelsen UP, North A, Heintz N, Omran H. Dysfunction of axonemal dynein heavy chain Mdnah5 inhibits ependymal flow and reveals a novel mechanism for hydrocephalus formation. *Hum Mol Genet* 2004;**13**:2133–2141.
- Kollmar M. Fine-tuning motile cilia and flagella: Evolution of the dynein motor proteins from plants to humans at high resolution. *Mol Biol Evol* 2016;**33**:3249–3267.
- Laiho A, Kotaja N, Gyenesei A, Sironen A. Transcriptome profiling of the murine testis during the first wave of spermatogenesis. *PLoS One* 2013;**8**:e61558.
- Liu C, Miyata H, Gao Y, Sha Y, Tang S, Xu Z, Whitfield M, Patrat C, Wu H, Duloust E et al. Bi-allelic DNAH8 variants lead to multiple morphological abnormalities of the sperm flagella and primary male infertility. *Am J Hum Genet* 2020;**107**:330–341.
- Loges NT, Antony D, Maver A, Deardorff MA, Güleç EY, Gezdirici A, Nöthe-Menchen T, Höben IM, Jelten L, Frank D et al. Recessive DNAH9 loss-of-function mutations cause laterality defects and subtle respiratory ciliary-beating defects. *Am J Hum Genet* 2018;**103**:995–1008.
- Loges NT, Olbrich H, Fenske L, Mussaffi H, Horvath J, Fliegauf M, Kuhl H, Baktai G, Peterffy E, Chodhari R et al. DNAI2 mutations cause primary ciliary dyskinesia with defects in the outer dynein arm. *Am J Hum Genet* 2008;**83**:547–558.
- Mitchell B, Jacobs R, Li J, Chien S, Kintner C. A positive feedback mechanism governs the polarity and motion of motile cilia. *Nature* 2007;**447**:97–101.
- Mukherjee S, Jansen V, Jikeli JF, Hamzeh H, Alvarez L, Dombrowski M, Balbach M, Strünker T, Seifert R, Kaupp UB et al. A novel biosensor to study camp dynamics in cilia and flagella. *Elife* 2016;**5**: e14052.
- Munro NC, Currie DC, Lindsay KS, Ryder TA, Rutman A, Dewar A, Greenstone MA, Hendry WF, Cole PJ. Fertility in men with primary ciliary dyskinesia presenting with respiratory infection. *Thorax* 1994;**49**:684–687.
- Munye MM, Shoemark A, Hirst RA, Delhove JM, Sharp TV, McKay TR, O'Callaghan C, Baines DL, Howe SJ, Hart SL. BMI-1 extends proliferative potential of human bronchial epithelial cells while retaining their mucociliary differentiation capacity. *Am J Physiol Lung Cell Mol Physiol* 2017;**312**:L258–L267.

- Nöthe-Menchen T, Wallmeier J, Pennekamp P, Höben IM, Olbrich H, Loges NT, Raidt J, Dougherty GW, Hjeij R, Dworniczak B et al. Randomization of left-right asymmetry and congenital heart defects: The role of DNAH5 in humans and mice. *Circ Genom Precis Med* 2019. 10.1161/CIRCGEN.119.002686.
- Oakberg EF. Duration of spermatogenesis in the mouse and timing of stages of the cycle of the seminiferous epithelium. *Am J Anat* 1956;**99**:507–516.
- Olbrich H, Cremers C, Loges NT, Werner C, Nielsen KG, Marthin JK, Philipson M, Wallmeier J, Pennekamp P, Menchen T et al. Loss-of-function GAS8 mutations cause primary ciliary dyskinesia and disrupt the nexin-dynein regulatory complex. *Am J Hum Genet* 2015;**97**:546–554.
- Olbrich H, Häffner K, Kispert A, Völkel A, Volz A, Sasmaz G, Reinhardt R, Hennig S, Lehrach H, Konietzko N et al. Mutations in DNAH5 cause primary ciliary dyskinesia and randomization of left-right asymmetry. *Nat Genet* 2002;**30**:143–144.
- Omran H, Kobayashi D, Olbrich H, Tsukahara T, Loges NT, Hagiwara H, Zhang Q, Leblond G, O'Toole E, Hara C et al. Ktu/PFI3 is required for cytoplasmic pre-assembly of axonemal dyneins. *Nature* 2008;**456**:611–616.
- Paff T, Loges NT, Aprea I, Wu K, Bakey Z, Haarman EG, Daniels JMA, Siermans EA, Bogunovic N, Dougherty GW et al. Mutations in PIH1D3 cause X-linked primary ciliary dyskinesia with outer and inner dynein arm defects. *Am J Hum Genet* 2017;**100**:160–168.
- Pazour GJ, Agrin N, Walker BL, Witman GB. Identification of predicted human outer dynein arm genes: Candidates for primary ciliary dyskinesia genes. *J Med Genet* 2006;**43**:62–73.
- Pennarun G, Escudier E, Chapelin C, Bridoux AM, Cacheux V, Roger G, Clément A, Goossens M, Amselem S, Duriez B. Loss-of-function mutations in a human gene related to Chlamydomonas reinhardtii dynein IC78 result in primary ciliary dyskinesia. *Am J Hum Genet* 1999;**65**:1508–1519.
- Pilatz A, Rusz A, Wagenlehner F, Weidner W, Altinkilic B. Reference values for testicular volume, epididymal head size and peak systolic velocity of the testicular artery in adult males measured by ultrasonography. *Ultraschall Med* 2013;**34**:349–354.
- Raidt J, Werner C, Menchen T, Dougherty GW, Olbrich H, Loges NT, Schmitz R, Pennekamp P, Omran H. Ciliary function and motor protein composition of human fallopian tubes. *Hum Reprod* 2015;**30**:2871–2880.
- Samant SA, Ogunkua O, Hui L, Fossella J, Pilder SH. T complex distorter 2 candidate gene, Dnahc8, encodes at least two testis-specific axonemal dynein heavy chains that differ extensively at their amino and carboxyl termini. *Dev Biol* 2002;**250**:24–43.
- Schindelin J, Arganda-Carreras I, Frise E, Kaynig V, Longair M, Pietzsch T, Preibisch S, Rueden C, Saalfeld S, Schmid B et al. Fiji: An open-source platform for biological-image analysis. *Nat Methods* 2012;**9**:676–682.
- Shah AS, Ben-Shahar Y, Moninger TO, Kline JN, Welsh MJ. Motile cilia of human airway epithelia are chemosensory. *Science* 2009;**325**:1131–1134.
- Sironen A, Shoemark A, Patel M, Loebinger MR, Mitchison HM. Sperm defects in primary ciliary dyskinesia and related causes of male infertility. *Cell Mol Life Sci* 2020;**77**:2029–2048.
- Sisson JH, Stoner JA, Ammons BA, Wyatt TA. All-digital image capture and whole-field analysis of ciliary beat frequency. *J Microsc* 2003;**211**:103–111.
- Spassky N, Meunier A. The development and functions of multiciliated epithelia. *Nat Rev Mol Cell Biol* 2017;**18**:423–436.
- Terré B, Lewis M, Gil-Gómez G, Han Z, Lu H, Aguilera M, Prats N, Roy S, Zhao H, Stracker TH. Defects in efferent duct multiciliogenesis underlie male infertility in GEMC1-, MCIDAS- or CCNO-deficient mice. *Development* 2019;**146**:dev162628.
- Vanaken GJ, Bassinet L, Boon M, Mani R, Honoré I, Papon JF, Cuppens H, Jaspers M, Lorent N, Coste A et al. Infertility in an adult cohort with primary ciliary dyskinesia: phenotype-gene association. *Eur Respir J* 2017;**50**:1700314.
- Wallmeier J. Mutationsanalyse im DNAH5-Gen bei Patienten mit Primärer Ziliärer Dyskinesie und bei Patienten mit kongenitalen Herzdefekten. [Dr. med.]. Albert-Ludwigs-Universität Freiburg im Breisgau, 2012.
- Wallmeier J, Al-Mutairi DA, Chen CT, Loges NT, Pennekamp P, Menchen T, Ma L, Shamseldin HE, Olbrich H, Dougherty GW et al. Mutations in CCNO result in congenital mucociliary clearance disorder with reduced generation of multiple motile cilia. *Nat Genet* 2014;**46**:646–651.
- Whitfield M, Thomas L, Bequignon E, Schmitt A, Stouvenel L, Montantin G, Tissier S, Duquesnoy P, Copin B, Chantot S et al. Mutations in DNAH17, encoding a sperm-specific axonemal outer dynein arm heavy chain, cause isolated male infertility due to asthenozoospermia. *Am J Hum Genet* 2019;**105**:198–212.
- Workman AD, Cohen NA. The effect of drugs and other compounds on the ciliary beat frequency of human respiratory epithelium. *Am J RhinolAllergy* 2014;**28**:454–464.
- World Health Organization. WHO laboratory manual for the examination and processing of human semen, 5th ed. Geneva: World Health Organization, 2010.
- Yuan S, Liu Y, Peng H, Tang C, Hennig GW, Wang Z, Wang L, Yu T, Klukovich R, Zhang Y et al. Motile cilia of the male reproductive system require miR-34/miR-449 for development and function to generate luminal turbulence. *Proc Natl Acad Sci U S A* 2019;**116**:3584–3593.